MECHANICAL MODELLING OF A BENT AXIS PUMP

Alessandro Roccatello and Nicola Nervegna

Politecnico di Torino - The Fluid Power Research Laboratory (FPRL)
Corso Duca degli Abruzzi 24, 10129 Torino, Italy
alessandro.roccatello@polito.it, nicola.nervegna@polito.it

Abstract

In the technical literature numerous studies are found focused on the mathematical modelling of mechanical aspects of swash plate axial piston pumps. Instead, bent axis pumps are rarely considered despite their widespread use in mobile and fixed applications. This research paper presents the mechanical model of a bent axis pump that simulates the dynamic behaviour of the main measurable quantities (e.g. the shaft torque) and the mutual forces in interacting components. The model is parametric and thus apt in predicting the influence of geometric design variables on pumps mechanical characteristics. A number of simulation analyses grounded on the presented model and on an ADAMS multibody approach are considered and contrasted one another and with experimental torque data for validation purposes.

Keywords: bent axis pump, modeling, simulation

1 Introduction

Over the last two decades the Fluid Power Research Laboratory (FPRL) has developed and validated simulation models for axial piston pumps and motors (Mancò et al., 2002), external and internal gear (gerotor) pumps (Fabiani et al., 1999), radial pistons (Caretto et al., 1996) as well as variable and fixed displacement vane pumps (Mancò et al., 2004). All have generally evolved in AMESim, elaborating proprietary libraries leading to an accurate prediction of the main hydraulic and mechanical quantities; recently, a multibody software code has also been proposed for the analysis of axial piston pumps (Roccatello et al., 2007). For this last pump family, models have been specifically developed for the swash plate category; this paper, instead, addresses modelling aspects of bent axis pumps (BAP). Since the hydraulic modelling has not required substantial modifications, being only adapted to the new pump topology (e.g. flow leakage between slippers and swash plate is absent), the present study will purposely focus on the mechanical modelling of the pump. The pertinent technical literature does not provide numerous resources about this topic: in Ivantysyn and Ivantysynova (2000) a description of the kinematics of BAP pumps is reported (considering various manufacturing solutions) that, in turn, supports the analysis of forces exchanged among components. These studies rely on scalar relations based on decomposition of forces and kinematic quantities along cartesian axes. In Osama et al. (2002) a partial description of piston kinematics for a BAP pump is described followed by studies on pump displacement controls. In Manring and Dong (2004) rotational matrices are used to express coordinate systems applied in the development of kinematic analysis of a swash plate pump; the analysis considers the existence of a secondary axis of rotation for the swash plate. Subsequently, results provided by kinematics are applied: piston velocity and acceleration are not attained through integration of the equation of motion but rather through time derivatives of analytical relations expressing its position. An analogous approach is followed in the present paper where kinematics is analysed first and all unknown reaction forces are determined thereafter. For this reason exchanged forces do not influence either position or velocity to account, for example, of microscale piston motion within the cylinder. Such an approach is detailed in Wieczorek and Ivantysynova (2002) where it is oriented to the study of tribologic phenomena. The present paper proposes a compact vector algebra approach; kinematics is initially described, stressing its higher complexity when compared to swash plate units. Subsequently, the mechanical modelling of the three principal components is discussed (piston, cylinder block, shaft) to evidence reciprocal forces. Fur-

This manuscript was received on 11 December 2008 and was accepted after revision for publication on 8 June 2009

thermore, the dynamic behaviour of interacting forces is documented and analysed trying to provide an explanation of existent relations between forces and piston kinematics. As to the shaft torque a comparison is shown that confronts simulated results with experimentally obtained data.

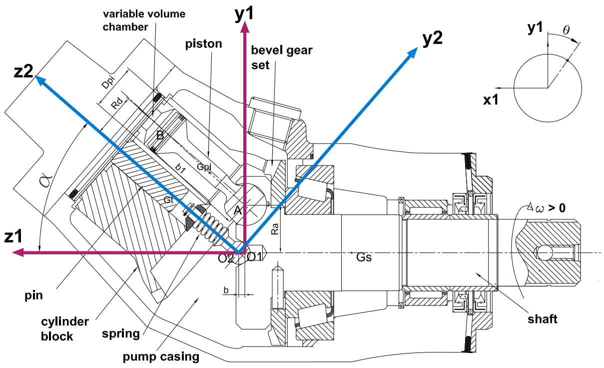

Fig. 1: *Section view of the bent axis pump, coordinate systems and main geometric quantities*

2 Pump Description and Operation

Generally, BAP pumps, when compared with swash plate units, are considered (Ivantysyn and Ivantysynova, 2000) more expensive and less compact, of more complex manufacturing and less adaptable to the various control strategies; nonetheless these units usually have a better total efficiency, are less sensitive to fluid contamination and allow a higher rotational speed. Different types of bent axis pumps are commercially available; for fixed displacement units, distinct techniques are accomplished to transfer shaft rotary motion to the cylinder block: cardan joints, connecting rodspistons and bevel gears. This last solution will be considered henceforth since it allows a larger tilt of the cylinder block (up to 45°, (Ivantysyn and Ivantysynova, 2000)), thus enhancing pump displacement; in addition, this solution is adopted by numerous manufacturers. Figure 1 shows a section view of the pump (Casappa Strada-BAP 63): a prime mover provides shaft rotation. The large cylindrical shaft boundary houses in spherical joints pistons that are, in turn, lodged within cylinders in the cylinder block. This is tilted of an angle a and rotates (guided by a cylindrical pin) at shaft angular velocity due to the bevel gears coupling. Variable volume chambers are isolated from pump casing through elastic rings that slip onto cylinders faces due to the influence of fluid pressure.

3 Pump Kinematics

For bent axis pumps, kinematic analysis is significantly more complex than for swash plate units. By way of example think of the piston centre of mass (CM): for swash plate pumps analytical relations describing coordinates (x,y,z) of CM are relatively simple to express since pistons undergo rotation about the shaft's axis and axial translation determined by swash plate's tilt (see (Roccatello et al., 2007)). Instead, for a bent axis unit, pistons are constrained by spherical joints integral with the shaft and by the collinearity of elastic ring centres with the cylinder axis. Consequently, pistons axes do not remain parallel but rather orbit in space in a more complex manner. Kinematic analysis has been grounded on four coordinate systems: geometric points of interest and coordinate systems being described by vectors and matrices, respectively.

Generally (Litvin et al., 2004), point M is represented in coordinate system $S_m(x_m, y_m, z_m)$ by the position vector:

$$ {}^{m}\boldsymbol{r} = \begin{bmatrix} x_m & y_m & z_m & 1 \end{bmatrix}^T \tag{1}$$

The same point M can be determined in coordinate system $S_n(x_n, y_n, z_n)$ by the position vector:

$$ {}^{n}\boldsymbol{r} = \begin{bmatrix} x_n & y_n & z_n & 1 \end{bmatrix}^T \tag{2}$$

with the matrix equation (position vectors being repre-sented with homogeneous coordinates):

$$ {}^{n}\boldsymbol{r} = \mathbf{M}_{nm}\,{}^{m}\boldsymbol{r} \tag{3}$$

Matrix $\mathbf{M}_{nm}$ is represented by:

$$ \mathbf{M}_{nm} = \begin{bmatrix} (\boldsymbol{i}_n\boldsymbol{i}_m) & (\boldsymbol{i}_n\boldsymbol{j}_m) & (\boldsymbol{i}_n\boldsymbol{k}_m) & x_n^{(O_m)} \\ (\boldsymbol{j}_n\boldsymbol{i}_m) & (\boldsymbol{j}_n\boldsymbol{j}_m) & (\boldsymbol{j}_n\boldsymbol{k}_m) & y_n^{(O_m)} \\ (\boldsymbol{k}_n\boldsymbol{i}_m) & (\boldsymbol{k}_n\boldsymbol{j}_m) & (\boldsymbol{k}_n\boldsymbol{k}_m) & z_n^{(O_m)} \\ 0 & 0 & 0 & 1 \end{bmatrix} \tag{4}$$

Subscript "nm" in the designation $\mathbf{M}_{nm}$ indicates that the coordinate transformation is performed from S_m to S_n. Here, $(\boldsymbol{i}_n, \boldsymbol{j}_n, \boldsymbol{k}_n)$ are the unit vectors of the axes of S_n; $(\boldsymbol{i}_m, \boldsymbol{j}_m, \boldsymbol{k}_m)$ are the unit vectors of the axes of S_m; (x_n, y_n, z_n) represent the coordinates of the origin O_m of S_m in coordinate system S_n (origin O_n). Dot products in matrix $\mathbf{M}_{nm}$ (e.g. $\boldsymbol{i}_n\boldsymbol{k}_m$) can be expressed through direction cosines or as an indexed sum of their components (e.g. $\boldsymbol{i}_{n,x}\boldsymbol{k}_{m,x}+\boldsymbol{i}_{n,y}\boldsymbol{k}_{m,y}+\boldsymbol{i}_{n,z}\boldsymbol{k}_{m,z}$).

The inverse coordinate transformation that determines the coordinates (x_m, y_m, z_m) taking as given coordinates (x_n, y_n, z_n) can be written as :

$$ {}^{m}\boldsymbol{r} = \mathbf{M}_{nm}\,{}^{m}\boldsymbol{r} \tag{5}$$

3.1 Coordinate Systems, Coordinate Transformations and Matrices

In concert with general principles recalled above, the analysis of pump kinematics, as presented hereafter, considers four coordinate systems that prove expedient in the development phase of governing equations. The chosen systems are identified as S_1, S_2, S_3 and S_4. Coordinate transformations and related matrices will now be introduced:

3.1.1 Coordinate Systems S_1 and S_2; Matrix $\mathbf{M}_{12}$

Coordinate systems S_1 (x_1, y_1, z_1) and S_2 (x_2, y_2, z_2) are fixed in space and indicated in Fig. 1. Worth of notice is the fact that their origins are separated by the distance b. The coordinate transformation from S_2 to S_1 is based on the matrix equation:

$$^{1}\boldsymbol{r} = \mathbf{M}_{12}\,{}^{2}\boldsymbol{r} \tag{6}$$

It is straightforward to write matrix and its inverse as follows:

$$\mathbf{M}_{12} = \begin{bmatrix} 1 & 0 & 0 & 0 \\ 0 & \cos\alpha & \sin\alpha & 0 \\ 0 & -\sin\alpha & \cos\alpha & b \\ 0 & 0 & 0 & 1 \end{bmatrix}$$
$$\mathbf{M}_{21} = \begin{bmatrix} 1 & 0 & 0 & 0 \\ 0 & \cos\alpha & -\sin\alpha & b\sin\alpha \\ 0 & \sin\alpha & \cos\alpha & -b\cos\alpha \\ 0 & 0 & 0 & 1 \end{bmatrix} \tag{7}$$

The coordinate transformation in transition from S_2 to S_1 is represented by the equations:

$$\begin{aligned} x_1 &= x_2 \\ y_1 &= y_2 \cdot \cos\alpha + z_2 \cdot \sin\alpha \\ z_1 &= -\, y_2 \cdot \sin\alpha + z_2 \cdot \cos\alpha + b \end{aligned} \tag{8}$$

3.1.2 Coordinate System S_3; Matrix $\mathbf{M}_{13}$

Coordinate system S_3, movable in space, has the origin at point A, centre of the spherical piston joint and axis $z3$ directed along the piston's axis from A to B, centre of the elastic ring (see Fig. 2).

Consider now point A that, constrained to rotate about the shaft's axis, describes in S_1 a circumference of radius Ra. Position vector ${}^{1}\boldsymbol{r}_{\mathrm{A}}$ is then written as (see Fig. 3).

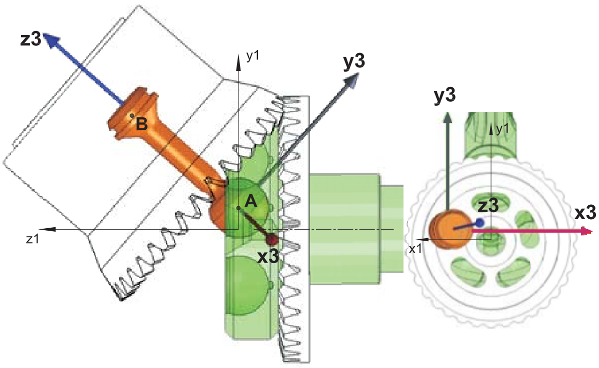

Fig. 2: *Coordinate systems S_3 and S_1*

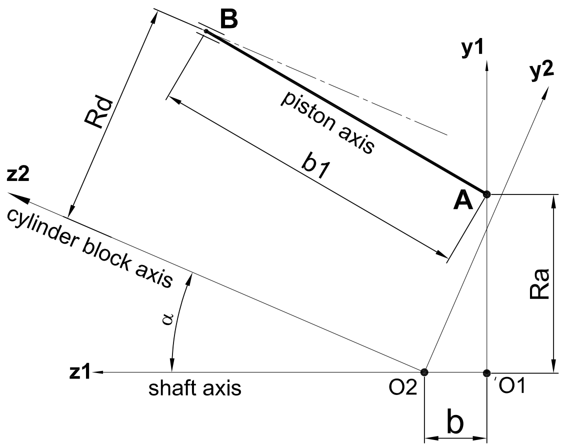

Fig. 3: *Approach to pump kinematics*

$${}^{1}\boldsymbol{r}_{\mathrm{B}} = \begin{bmatrix} -Ra\sin\vartheta & Ra\cos\vartheta & 0 & 1 \end{bmatrix}^{\mathrm{T}} \tag{9}$$

In turn position vector ${}^{1}\boldsymbol{r}_{\mathrm{B}}$ of point B in coordinate system S_1 can be formally expressed by the matrix equation:

$${}^{1}\boldsymbol{r}_{\mathrm{B}} = \mathbf{M}_{12}\,{}^{2}\boldsymbol{r}_{\mathrm{B}} \tag{10}$$

where:

$${}^{2}\boldsymbol{r}_{\mathrm{B}} = \begin{bmatrix} -Rd\sin\vartheta \\ Rd\cos\vartheta \\ {}^{2}z_{\mathrm{A}} + \sqrt{{}^{2}z_{\mathrm{A}} - a_1} \\ 1 \end{bmatrix} \tag{11}$$

being:

$$a_1 = \left({}^{2}x_{\mathrm{B}} - {}^{2}x_{\mathrm{A}}\right)^2 + \left({}^{2}y_{\mathrm{B}} - {}^{2}y_{\mathrm{A}}\right)^2 + {}^{2}z_{\mathrm{A}}{}^{2} - b_1^2 \tag{12}$$

Having identified the position of points A and B, it is possible to express unit vectors of S_3 in S_1; through Eq. 9 and 11, the unit vector of axis $z3$ in S_1 is:

$${}^{1}\boldsymbol{k}_3 = \frac{\left({}^{1}\boldsymbol{r}_{\mathrm{B}} - {}^{1}\boldsymbol{r}_{\mathrm{A}}\right)}{\left|{}^{1}\boldsymbol{r}_{\mathrm{B}} - {}^{1}\boldsymbol{r}_{\mathrm{A}}\right|} \tag{13}$$

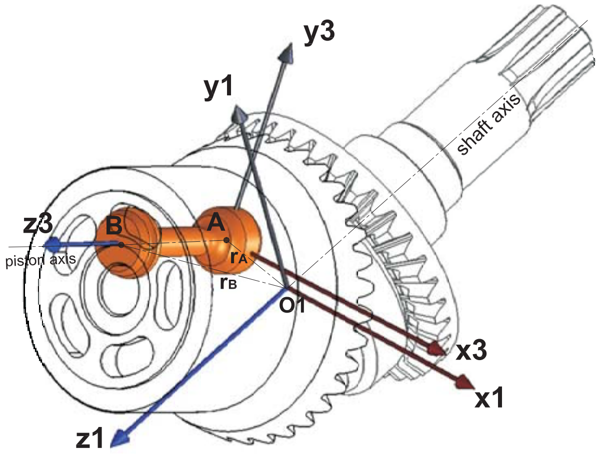

Fig. 4: *Coordinate systems S_3 and S_1*

$${}^{1}\boldsymbol{j}_3\,{}^{1}\boldsymbol{k}_3 = {}^{1}j_{3,\mathrm{x}}\,{}^{1}k_{3,\mathrm{x}} + {}^{1}j_{3,\mathrm{y}}\,{}^{1}k_{3,\mathrm{y}} + {}^{1}j_{3,\mathrm{z}}\,{}^{1}k_{3,\mathrm{z}} = 0 \tag{14}$$

The unit vector of axis $y3$ (${}^{1}\boldsymbol{j}_3 = \begin{bmatrix} {}^{1}j_{3,\mathrm{x}} & {}^{1}j_{3,\mathrm{y}} & {}^{1}j_{3,\mathrm{z}} \end{bmatrix}^{\mathrm{T}}$) has the following properties: (a) is normal to ${}^{1}\boldsymbol{k}_3$; (b) lays on a plane parallel to plane ($y1$, $z1$); (c) has a unitary module. While (a) is equivalent to the following scalar relation (dot product between ${}^{1}\boldsymbol{j}_3$ and ${}^{1}\boldsymbol{k}_3$ equal to zero) property (b) sets to zero the component of the unit vector ${}^{1}\boldsymbol{j}_3$ along the x axis:

$${}^{1}\boldsymbol{j}_{3,\,\mathrm{x}} = 0 \tag{15}$$

From (c) immediately follows:

$${}^{1}\boldsymbol{j}_{3,\,\mathrm{x}}{}^{2} + {}^{1}\boldsymbol{j}_{3,\,\mathrm{y}}{}^{2} + {}^{1}\boldsymbol{j}_{3,\,\mathrm{z}}{}^{2} = 1 \tag{16}$$

Equations 14 to 16 in three unknowns (${}^{1}\boldsymbol{j}_{3,\mathrm{x}}$, ${}^{1}\boldsymbol{j}_{3,\mathrm{y}}$, ${}^{1}\boldsymbol{j}_{3,\mathrm{z}}$) lead to:

$$
\begin{aligned}
&{}^1\boldsymbol{j}_{3,y} = \left(-\frac{{}^1\boldsymbol{k}_{3,z}}{{}^1\boldsymbol{k}_{3,y}}\right){}^1\boldsymbol{j}_{3,z} \\
&{}^1\boldsymbol{j}_{3,z} = \pm\sqrt{\frac{1}{1+\dfrac{{}^1\boldsymbol{k}_{3,z}^{\,2}}{{}^1\boldsymbol{k}_{3,y}^{\,2}}}} \\
&{}^1\boldsymbol{j}_{3,x} = 0
\end{aligned}
\tag{17}
$$

where the positive sign is selected to define the positive direction of ${}^1\boldsymbol{j}_3$. The unit vector of the *x3* axis is derived from knowledge of the other two: ${}^1\boldsymbol{i}_3 = {}^1\boldsymbol{j}_3 \wedge {}^1\boldsymbol{k}_3$ Matrix $\mathbf{M}_{13}$, is written as follows:

$$
\mathbf{M}_{13} = \begin{bmatrix} (\boldsymbol{i}_1\boldsymbol{i}_3) & (\boldsymbol{i}_1\boldsymbol{j}_3) & (\boldsymbol{i}_1\boldsymbol{k}_3) & x_1^{(O_3)} \\ (\boldsymbol{j}_1\boldsymbol{i}_3) & (\boldsymbol{j}_1\boldsymbol{j}_3) & (\boldsymbol{j}_1\boldsymbol{k}_3) & y_1^{(O_3)} \\ (\boldsymbol{k}_1\boldsymbol{i}_3) & (\boldsymbol{k}_1\boldsymbol{j}_3) & (\boldsymbol{k}_1\boldsymbol{k}_3) & z_1^{(O_3)} \\ 0 & 0 & 0 & 1 \end{bmatrix}
= \begin{bmatrix} {}^1\boldsymbol{i}_{3,x} & {}^1\boldsymbol{j}_{3,x} & {}^1\boldsymbol{k}_{3,x} & {}^1\boldsymbol{r}_{A,x} \\ {}^1\boldsymbol{i}_{3,y} & {}^1\boldsymbol{j}_{3,y} & {}^1\boldsymbol{k}_{3,y} & {}^1\boldsymbol{r}_{A,y} \\ {}^1\boldsymbol{i}_{3,z} & {}^1\boldsymbol{j}_{3,z} & {}^1\boldsymbol{k}_{3,z} & {}^1\boldsymbol{r}_{A,z} \\ 0 & 0 & 0 & 1 \end{bmatrix}
\tag{18}
$$

where $(\boldsymbol{i}_1, \boldsymbol{j}_1, \boldsymbol{k}_1)$ are the unit vectors of the axes of S_1; $(\boldsymbol{i}_3, \boldsymbol{j}_3, \boldsymbol{k}_3)$ are the unit vectors of the axes of S_3; (*x1*, *y1*, *z1*) represent the coordinates of the origin O_3 of S_3 in coordinate system S_1 (origin O_1).

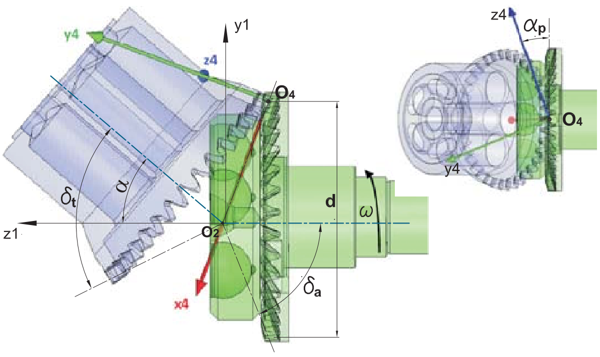

Fig. 5: *Coordinate systems S_4 and S_1*

In the analysis *N* coordinate systems (S_{3k}, k = 1...*N*) are effectively considered each integral with the corresponding piston *k* (see Fig. 2) featuring points A_k and B_k: the aim being that of expressing with relative ease some involved forces; e.g., that exchanged between piston and shaft and directed along the piston's axis movable in space. Coordinate systems are identified by their different angular position: $\vartheta_k = \vartheta - (k - 1)\cdot 2\pi / N$[1]. Matrix $\mathbf{M}_{13}$ presented above (18) is expanded in analytical relations that, owing to their considerable length, are here omitted; however, a Matlab code is provided in the Appendix that allows the generation of the complete symbolic expression.

[1] To simplify notations, while expressing points *A*, *B* and matrix $\mathbf{M}_{13}$, subscript *k* has been deliberately omitted. In (9) and (11) coordinate ϑ should, in fact, read ϑ_k, thus identifiying *N* couples of points *A* and *B* as well as *N* coordinate systems S_3. Pistons are numbered sequentially in the CCW direction: hence, piston $k + 1$ follows *k* if the pump rotates clockwise.

3.1.3 Coordinate System S_4; Matrix $\mathbf{M}_{14}$

A last fixed coordinate system S_4 has been introduced *O4* (*x4*, *y4*, *z4*), to identify the axis *z4* that corresponds to the line of action of the force exchanged in the bevel gears mating: this being convenient while writing equilibrium equations and more specifically the reaction force $\boldsymbol{R}_{cs}$ between cylinder block and shaft through the mating gears. In the left portion of Fig. 5 it can be observed that the driving gear is integral with the shaft while the driven with the cylinder block. Axes of rotation are tilted of an angle α, gears feature the same number of teeth and have equal pitch cones angles ($\delta_a = \delta_t$). Under the hypotheses that (i) the condition of meshing involves only one pair of teeth (Jacazio and Piombo, 1997), (ii) that gears are in point contact and (iii) that the exchanged force $\boldsymbol{R}_{cs}$ is applied at *O4*, midpoint of teeth faces on the conical pitch surface, the position vector of the origin *O4* in coordinate system S_1 follows:

$$
{}^1\boldsymbol{r}_{O4} = \begin{bmatrix} 0 & \dfrac{mZ}{2} & -\dfrac{mZ}{2}\cot\delta_a + b & 1 \end{bmatrix}^T \rightarrow \tag{19}
$$

being the pitch cone diameter at the contact point d = mZ. It is then possible to write:

$$
{}^2\boldsymbol{r}_{O4} = \mathbf{M}_{21}\,{}^1\boldsymbol{r}_{O4} \tag{20}
$$

Knowledge of ${}^2\boldsymbol{r}_{O4}$ allows to express the three components of unit vectors *x4*, *y4* and *z4* as follows:

- The unit vector of *x4* in S_1 (${}^1\boldsymbol{I}_i$) is oriented from *O4* to *O2* and consequently:

$$
{}^2\boldsymbol{i}_4 = -\frac{{}^2\boldsymbol{r}_{O4}}{\left|{}^2\boldsymbol{r}_{O4}\right|} \rightarrow {}^1\boldsymbol{i}_4 = \mathbf{M}_{12}\,{}^2\boldsymbol{i}_4 \tag{21}
$$

- The unit vector of *z4* in S_1 (${}^1\boldsymbol{k}_4$) has a tilt equal to the pressure angle (α_p) and can be defined as follows:

$$
{}^1\boldsymbol{k}_4 = \begin{bmatrix} -\cos\alpha_p \; sign(\omega) \\ \sin\alpha_p \;\cos\delta \; sign(\omega) \\ \sin\alpha_p \;\sin\delta \; sign(\omega) \end{bmatrix} \tag{22}
$$

where the operator sign (ω) accounts for the possibility of reversing pump rotational speed.

- The unit vector of *y4* in S_1 (${}^1\boldsymbol{j}_4$) is, by definition: ${}^1\boldsymbol{j}_4 = {}^1\boldsymbol{k}_4 \wedge {}^1\boldsymbol{i}_4$ Matrix $\mathbf{M}_{14}$, is written as follows: (cfr. (4)):

$$
\mathbf{M}_{14} = \begin{bmatrix} (\boldsymbol{i}_1\boldsymbol{i}_4) & (\boldsymbol{i}_1\boldsymbol{j}_4) & (\boldsymbol{i}_1\boldsymbol{k}_4) & x_1^{(O_4)} \\ (\boldsymbol{j}_1\boldsymbol{i}_4) & (\boldsymbol{j}_1\boldsymbol{j}_4) & (\boldsymbol{j}_1\boldsymbol{k}_4) & y_1^{(O_4)} \\ (\boldsymbol{k}_1\boldsymbol{i}_4) & (\boldsymbol{k}_1\boldsymbol{j}_4) & (\boldsymbol{k}_1\boldsymbol{k}_4) & z_1^{(O_4)} \\ 0 & 0 & 0 & 1 \end{bmatrix}
= \begin{bmatrix} {}^1\boldsymbol{i}_{4,x} & {}^1\boldsymbol{j}_{4,x} & {}^1\boldsymbol{k}_{4,x} & 0 \\ {}^1\boldsymbol{i}_{4,y} & {}^1\boldsymbol{j}_{4,y} & {}^1\boldsymbol{k}_{4,y} & \dfrac{mZ}{2} \\ {}^1\boldsymbol{i}_{4,z} & {}^1\boldsymbol{j}_{4,z} & {}^1\boldsymbol{k}_{4,z} & -\dfrac{mZ}{2}\cot\delta_a + b \\ 0 & 0 & 0 & 1 \end{bmatrix}
\tag{23}
$$

This also leads to: $\mathbf{M}_{24} = \mathbf{M}_{21}\mathbf{M}_{14}$

4 Mechanical Modelling

4.1 Piston Model

Figure 6 shows a generic piston k and applied external forces.

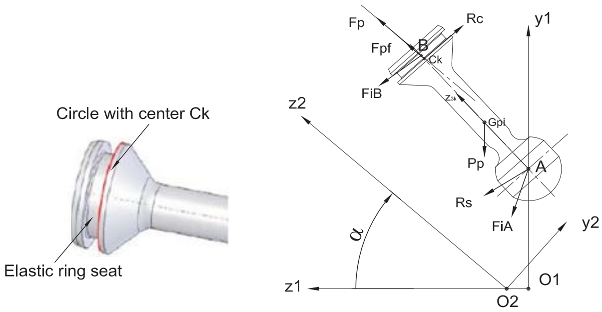

Fig. 6: *Free body diagram of the piston*

4.1.1 Known Forces Acting on Piston

- $\boldsymbol{F}_{\mathrm{p,k}}$: force originated by fluid pressure acting along axis *z2:*

$$ {}^{2}\boldsymbol{F}_{\mathrm{p,k}} = \begin{bmatrix} 0 & 0 & -\mathrm{p_k}\dfrac{\pi D_{\mathrm{pi}}^2}{4} \end{bmatrix}^{\mathrm{T}} \tag{24} $$

- $\boldsymbol{F}_{\mathrm{pf,k}}$: friction force:

$$ {}^{2}\boldsymbol{F}_{\mathrm{pf,k}} = \begin{bmatrix} 0 & 0 & -\left|\boldsymbol{F}_{\mathrm{pf,k}}\right| \mathrm{sign}\left({}^{2}v_{\mathrm{Bk,\,z}}\right) \end{bmatrix}^{\mathrm{T}} \tag{25} $$

in general $\left|\boldsymbol{F}_{\mathrm{pf,k}}\right|$ depends on point $\mathrm{B_k}$ velocity.

- $\boldsymbol{P}_{\mathrm{p,\,k}}$: piston weight:

$$ \begin{aligned} {}^{1}\boldsymbol{P}_{\mathrm{p,k}} &= \begin{bmatrix} 0 & -\mathrm{m}_{pi}\mathrm{g} & 0 \end{bmatrix}^{\mathrm{T}} \\ {}^{2}\boldsymbol{P}_{\mathrm{p,k}} &= \mathbf{M}_{12}\,{}^{1}\boldsymbol{P}_{\mathrm{p,k}} \end{aligned} \tag{26} $$

- $\boldsymbol{F}_{\mathrm{iA,k}}$ and $\boldsymbol{F}_{\mathrm{iB,k}}$: inertia forces. Two contributions are considered since piston mass is, by hypothesis, lumped in points A_{k} and B_{k}. This assumption avoids calculations of terms dependent on angular acceleration $(\dot{\omega})$ and of correspondent inertial contributions. In the Appendix it is shown that this simplification does not give rise to significant differences in attained results. Thus, piston mass m_{pi} is divided, into two generally different portions: m_{A} at point A_{k} and m_{B} at point B_{k} as follows:

$$ \begin{aligned} m_{\mathrm{A}} + m_{\mathrm{B}} &= m_{\mathrm{pi}} \\ m_{\mathrm{A}} &= \chi\, m_{\mathrm{pi}} \end{aligned} \tag{27} $$

Taking the time derivatives of Eq. 9 and 11, velocity and acceleration of points $\mathrm{A_k}$ e $\mathrm{B_k}$ are determined. Consequently:

$$ {}^{2}\boldsymbol{F}_{\mathrm{iA,k}} = m_{\mathrm{A}}\,{}^{2}\boldsymbol{a}_{\mathrm{Ak}}\;{}^{2}\boldsymbol{F}_{\mathrm{iB,\,k}} = -\,m_{\mathrm{B}} -{}^{2}\boldsymbol{a}_{\mathrm{Bk}} \tag{28} $$

4.1.2 Unknown Reactions on Piston

- $\boldsymbol{R}_{\mathrm{s,k}}$: reaction force on piston (point A_{k}) from shaft; mating of the two components has been modelled with a spherical joint that removes three translational DOF. Three reaction forces are then unknown:

$$ {}^{2}\boldsymbol{R}_{\mathrm{s,k}} = \begin{bmatrix} {}^{2}R_{\mathrm{s,kx}} & {}^{2}R_{\mathrm{s,ky}} & {}^{2}R_{\mathrm{s,kz}} \end{bmatrix}^{\mathrm{T}} \tag{29} $$

Note that in the N coordinate systems S_3, with origins in the spherical piston joints, reaction (${}^{3}\boldsymbol{R}_{\mathrm{s,k}}$) has a single component along piston axis (k_3). Position vector ${}^{2}\boldsymbol{R}_{\mathrm{s,k}}$ can be written in S_3 as ${}^{3}\boldsymbol{R}_{\mathrm{s,k}}$ through matrix $\mathbf{M}_{23\mathrm{k}} = \mathbf{M}_{21}\,\mathbf{M}_{13\mathrm{k}}$.

- $\boldsymbol{R}_{\mathrm{c,k}}$: reaction force on piston (point C_{k}) from cylinder block; the assumption is here made that the piston may contact the internal cylinder face in a generic point belonging to the circumference with centre $\boldsymbol{C}_{\mathbf{k}}$ (see Fig. 6). In this respect it should be noticed that the elastic ring is not integral with the piston and, as a consequence, the latter may lean onto the cylinder in a point that differs from the centre of the sphere defining the external surface of the ring (at point B_{k})[2]. In coordinate system S_2 only two unknown reaction forces exist since no contribution is to be accounted along the *z2* axis[3].

$$ {}^{2}\boldsymbol{R}_{\mathrm{c,k}} = \begin{bmatrix} {}^{2}R_{\mathrm{c,\,kx}} & {}^{2}R_{\mathrm{c,\,ky}} & 0 \end{bmatrix}^{\mathrm{T}} \tag{30} $$

4.1.3 Equilibrium Equations

Piston translational and rotational (about *O2*) equilibrium equations in coordinate system S_2 are written, in vector notation, as follows[4]:

$$ \begin{aligned} &{}^{2}\boldsymbol{F}_{\mathrm{p,k}} + {}^{2}\boldsymbol{F}_{\mathrm{pf,k}} + {}^{2}\boldsymbol{P}_{\mathrm{p,k}} + {}^{2}\boldsymbol{F}_{\mathrm{iA,k}} + \ldots \\ &\ldots + {}^{2}\boldsymbol{F}_{\mathrm{iB,k}} + {}^{2}\boldsymbol{R}_{\mathrm{s,k}} + {}^{2}\boldsymbol{R}_{\mathrm{c,k}} = 0 \end{aligned} \tag{31} $$

$$ \begin{aligned} &{}^{2}\boldsymbol{r}_{\mathrm{B}} \wedge {}^{2}\boldsymbol{F}_{\mathrm{p,k}} + {}^{2}\boldsymbol{r}_{\mathrm{B}} \wedge {}^{2}\boldsymbol{F}_{\mathrm{pf,k}} + {}^{2}\boldsymbol{r}_{\mathrm{Gpi}} \wedge {}^{2}\boldsymbol{P}_{\mathrm{p,k}} + \ldots \\ &\ldots + {}^{2}\boldsymbol{r}_{\mathrm{A}} \wedge {}^{2}\boldsymbol{F}_{\mathrm{inA,k}} + {}^{2}\boldsymbol{r}_{\mathrm{B}} \wedge {}^{2}\boldsymbol{F}_{\mathrm{inB,k}} + \ldots \\ &\ldots + {}^{2}\boldsymbol{r}_{\mathrm{A}} \wedge {}^{2}\boldsymbol{R}_{\mathrm{s,k}} + {}^{2}\boldsymbol{r}_{\mathrm{C_k}} \wedge {}^{2}\boldsymbol{R}_{\mathrm{c,k}} = 0 \end{aligned} \tag{32} $$

From Eq. 31 and 32 a linear system of five equations in five unknowns (${}^{2}R_{\mathrm{s,kx}}$ ${}^{2}R_{\mathrm{s,ky}}$ ${}^{2}R_{\mathrm{s,kz}}$ ${}^{2}R_{\mathrm{c,kx}}$ ${}^{2}R_{\mathrm{c,ky}}$) is obtained:

$$ \mathbf{A_p}\,\mathbf{X_p} = \mathbf{B_p} \tag{33} $$

4.2 Shaft Model

Figure 7 shows the shaft and applied external forces. Equilibrium equations will be written in coordinate system S_1. The shaft and the driving bevel gear will be considered as a single rigid body.

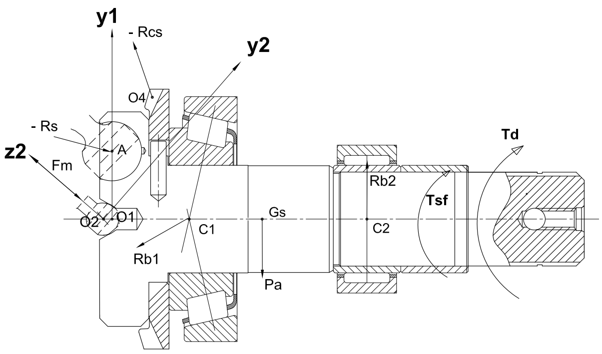

Fig. 7: *Shaft free body diagram*

[2] The elastic ring seals the variable volume chamber while the piston contacts the cylinder in a point of the circumference centred in C_{k}.

[3] Friction, expressed previously, is here considered as a known force.

[4] To simplify notation A_{k} and B_{k} are written as A and B

4.2.1 Known Forces Acting on Shaft

- $\boldsymbol{F}_{\mathrm{m}}$: spring force; in coordinate system S_2 has a single component (along $z2$):

$$ {}^{2}\boldsymbol{F}_{\mathrm{m}} = \begin{bmatrix} 0 & 0 & {}^{2}F_{\mathrm{m,z}} \end{bmatrix}^{\mathrm{T}} \qquad {}^{1}\boldsymbol{F}_{\mathrm{m}} = \mathbf{M}_{12}\,{}^{2}\boldsymbol{F}_{\mathrm{m}} \tag{34} $$

where ${}^{2}\boldsymbol{F}_{\mathrm{m,z}}$ is the spring force magnitude, determined from elastic and geometric properties.

- ${}^{2}\boldsymbol{R}_{\mathrm{s,k}}$: this reaction has already been obtained in S_1 in the piston model; hence it is now a known force:

$$ -{}^{2}\boldsymbol{R}_{\mathrm{s,k}} = \begin{bmatrix} -{}^{2}R_{\mathrm{s,kx}} & -{}^{2}R_{\mathrm{s,ky}} & -{}^{2}R_{\mathrm{s,kz}} \end{bmatrix}^{\mathrm{T}} \\ \rightarrow {}^{1}\boldsymbol{R}_{\mathrm{s,k}} = \mathbf{M}_{12}\,{}^{2}\boldsymbol{R}_{\mathrm{s,k}} \tag{35} $$

- $\boldsymbol{R}_{\mathrm{cs}}$: reaction force on the shaft from the cylinder block through the bevel gears mating. This reaction will be evaluated in the cylinder block model and can be considered here as a known force with three components in coordinate system S_1:

$$ -{}^{1}\boldsymbol{R}_{\mathrm{cs}} = \begin{bmatrix} -{}^{1}R_{\mathrm{cs,\,x}} & -{}^{1}R_{\mathrm{cs,\,y}} & -{}^{1}R_{\mathrm{cs,\,z}} \end{bmatrix}^{\mathrm{T}} \tag{36} $$

- $\boldsymbol{P}_{\mathrm{s}}$: shaft weight:

$$ {}^{1}\boldsymbol{P}_{\mathrm{s}} = [0 \;\; -m_{\mathrm{s}}g \;\; 0]^{\mathrm{T}} \tag{37} $$

- $\boldsymbol{T}_{\mathrm{sf}}$: friction torque on the shaft. Two parameters (C_{s}) and (C_{t}) are introduced to consider viscous torque losses and losses proportional to torque T_{d} required by the pump to keep the shaft turning at constant angular velocity:

$$ {}^{1}\boldsymbol{T}_{\mathrm{sf}} = \begin{bmatrix} 0 & 0 & -T_{\mathrm{d}}\left(1-C_{\mathrm{t}}\right) - C_{\mathrm{s}}\omega \end{bmatrix}^{\mathrm{T}} \tag{38} $$

4.2.2 Unknown Reactions on Shaft

- $\boldsymbol{R}_{\mathrm{b1}}$: reaction force (point C1) from tapered roller bearing. In S_1 we will generally observe three components:

$$ {}^{1}\boldsymbol{R}_{\mathrm{b1}} = \begin{bmatrix} {}^{1}R_{\mathrm{b1,\,x}} & {}^{1}R_{\mathrm{b1,\,y}} & {}^{1}R_{\mathrm{b1,\,z}} \end{bmatrix}^{\mathrm{T}} \tag{39} $$

- $\boldsymbol{R}_{\mathrm{b2}}$: reaction force (point C_2) from cylindrical roller bearing. In this case the component along $z1$ is missing, therefore:

$$ {}^{1}\boldsymbol{R}_{\mathrm{b2}} = \begin{bmatrix} {}^{1}R_{\mathrm{b2,\,x}} & {}^{1}R_{\mathrm{b2,\,y}} & 0 \end{bmatrix}^{\mathrm{T}} \tag{40} $$

- $\boldsymbol{T}_{\mathrm{ex}}$: drive torque required from prime mover:

$$ {}^{1}\boldsymbol{T}_{\mathrm{ex}} = \begin{bmatrix} 0 & 0 & {}^{1}T_{\mathrm{d}} \end{bmatrix}^{\mathrm{T}} \tag{41} $$

4.2.3 Equilibrium Equations

Shaft translational and rotational (about $O1$) equilibrium equations in coordinate system S_1 are written, in vector notation, as follows:

$$ {}^{1}\boldsymbol{F}_{\mathrm{m}} + \sum_{\mathrm{k}}\left(-{}^{1}\boldsymbol{R}_{\mathrm{s,\,k}}\right) - {}^{1}\boldsymbol{R}_{\mathrm{cs}} + {}^{1}\boldsymbol{P}_{\mathrm{s}} + {}^{1}\boldsymbol{R}_{\mathrm{b1}} + {}^{1}\boldsymbol{R}_{\mathrm{b2}} = 0 \tag{42} $$

$$ {}^{1}\boldsymbol{r}_{02} \wedge {}^{1}\boldsymbol{F}_{\mathrm{m}} + \sum_{\mathrm{k}} {}^{1}\boldsymbol{r}_{\mathrm{Ak}} \wedge \left(-{}^{1}\boldsymbol{R}_{\mathrm{s,\,k}}\right) + {}^{1}\boldsymbol{r}_{04} \wedge \left(-{}^{1}\boldsymbol{R}_{\mathrm{cs}}\right) + \ldots \\ {}^{1}\boldsymbol{r}_{\mathrm{Gs}} \wedge {}^{1}\boldsymbol{P}_{\mathrm{s}} + {}^{1}\boldsymbol{T}_{\mathrm{sf}} + {}^{1}\boldsymbol{T}_{\mathrm{ex}} + \ldots \\ \ldots + {}^{1}\boldsymbol{r}_{\mathrm{c2}} \wedge {}^{1}\boldsymbol{R}_{\mathrm{b2}} + {}^{1}\boldsymbol{r}_{\mathrm{c1}} \wedge {}^{1}\boldsymbol{R}_{\mathrm{b2}} = 0 \tag{43} $$

The system takes the following matrix notation (six unknowns ${}^{1}\boldsymbol{R}_{\mathrm{b1,x}}$ ${}^{1}\boldsymbol{R}_{\mathrm{b1,y}}$ ${}^{1}\boldsymbol{R}_{\mathrm{b1,z}}$ ${}^{1}\boldsymbol{R}_{\mathrm{b2,x}}$ ${}^{1}\boldsymbol{R}_{\mathrm{b2,y}}$ ${}^{1}\boldsymbol{T}_{\mathrm{d}}$):

$$ \mathbf{A_a}\,\mathbf{X_a} = \mathbf{B_a} \tag{44} $$

4.3 Cylinder Block Model

Figure 8 shows the cylinder block and applied external forces. Equilibrium equations will be written in coordi-nate system S_2.

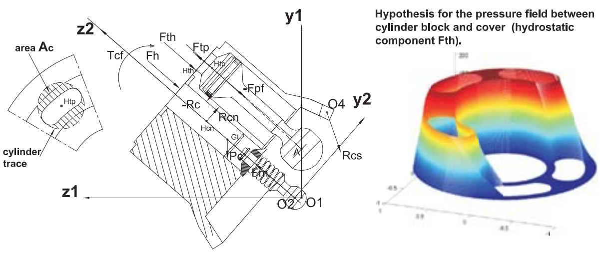

Fig. 8: *cylinder block free body diagram*

4.3.1 Known Forces Acting on Cylinder Block

- $\boldsymbol{F}_{\mathrm{m}}$: spring force; in coordinate system S_2 has a single component (along $z2$):

$$ {}^{2}\boldsymbol{F}_{\mathrm{m}} = \begin{bmatrix} 0 & 0 & {}^{2}F_{\mathrm{m,z}} \end{bmatrix}^{\mathrm{T}} \tag{45} $$

- $\boldsymbol{F}_{\mathrm{pf,k}}$: friction force (see (25)).
- $\boldsymbol{P}_{\mathrm{c}}$: cylinder block weight. Active along the $y1$ axis:

$$ {}^{1}\boldsymbol{P}_{\mathrm{c}} = \begin{bmatrix} 0 & -m_{\mathrm{c}}g & 0 \end{bmatrix}^{\mathrm{T}} \qquad {}^{2}\boldsymbol{P}_{\mathrm{c}} = \mathbf{M}_{21}\,{}^{1}\boldsymbol{P}_{\mathrm{c}} \tag{46} $$

- $\boldsymbol{T}_{\mathrm{cf}}$: friction torque on cylinder block. By accounting for the viscous component only:

$$ {}^{2}\boldsymbol{T}_{\mathrm{cf}} = \begin{bmatrix} 0 & 0 & -C_{\mathrm{c}}\omega \end{bmatrix}^{\mathrm{T}} \tag{47} $$

- ${}^{2}\boldsymbol{F}_{\mathrm{tp,k}}$: force, originated by fluid pressure within the cylinder, pushing the cylinder block against the pump cover; it acts along axis $z2$ at point $H_{\mathbf{tp,k}}$:

$$ {}^{2}\boldsymbol{F}_{\mathrm{tp,k}} = \begin{bmatrix} 0 & 0 & {}^{2}F_{\mathrm{tp,kz}} \end{bmatrix}^{\mathrm{T}} \tag{48} $$

where ${}^{2}\boldsymbol{F}_{\mathrm{tp,kz}} = \boldsymbol{A}_{\mathrm{c}}\,\boldsymbol{p}_{\mathrm{k}}$ and $\boldsymbol{A}_{\mathrm{c}}$ being shown in Fig. 8.

- ${}^{2}\boldsymbol{F}_{\mathrm{th}}$: force, originated by fluid pressure, pulling the cylinder block away from the cover. The assumption is here made that the pressure field, consequent to fluid pressure in cylinders, evolves linearly on sealing lips as specifically indicated in Fig. 8. This determines (${}^{2}\boldsymbol{F}_{\mathrm{th,z}}$) and its point of application ($\boldsymbol{H}_{\mathrm{th}}$).

$$ {}^{2}\boldsymbol{F}_{\mathrm{th}} = \begin{bmatrix} 0 & 0 & {}^{2}F_{\mathrm{th,z}} \end{bmatrix}^{\mathrm{T}} \tag{49} $$

- $\boldsymbol{R}_{\mathrm{c,k}}$: force on cylinder block (point $\mathbf{C_k}$) from piston. A known force already evaluated (see(30)):

$$ -{}^{2}\boldsymbol{R}_{\mathrm{c,k}} = \begin{bmatrix} -{}^{2}R_{\mathrm{c,\,kx}} & -{}^{2}R_{\mathrm{c,\,ky}} & 0 \end{bmatrix}^{\mathrm{T}} \tag{50} $$

4.3.2 Unknown Reactions on Cylinder Block

- $\boldsymbol{F}_{\mathrm{h}}$: hydrodynamic force, originated by fluid velocity and pressure, that pulls the cylinder block away from the cover; by assumption $\boldsymbol{F}_{\mathrm{h}}$ acts along axis $z2$ and arbitrates the axial equilibrium of the cylinder block:

$$ {}^{2}\boldsymbol{F}_{\mathrm{h}} = \begin{bmatrix} 0 & 0 & {}^{2}F_{\mathrm{h,z}} \end{bmatrix}^{\mathrm{T}} \tag{51} $$

However, it should be observed that such a force is not applied on the cylinder block axis but rather in a point of coordinates ($x2$, $y2$) = (x_{h}, y_{h}) to be so identified to guarantee its equilibrium also in reference to tilting moments about axes *x2* and *y2*.

Beside $\boldsymbol{F}_\mathrm{h}$ two unknown moments should then be considered.

- $\boldsymbol{T}_\mathrm{h}$: moment of force $\boldsymbol{F}_\mathrm{h}$ due to its offset position from axis *z2*:

$$ {}^2\boldsymbol{T}_\mathrm{h} = \left[{}^2T_\mathrm{h,x} \quad {}^2T_\mathrm{h,y} \quad 0 \right]^\mathrm{T} \tag{52} $$

the following equations correlate involved quantities:

$$ \mathbf{x_h} = \frac{{}^2T_\mathrm{h,y}}{-{}^2F_\mathrm{h,z}} \qquad \mathbf{y_h} = \frac{{}^2T_\mathrm{h,x}}{{}^2F_\mathrm{h,z}} \tag{53} $$

- $\boldsymbol{R}_\mathrm{cn}$: reaction force exerted by the pin; active in the radial direction at the mean contact point ($\boldsymbol{H}_\mathrm{cn}$):

$$ {}^2\boldsymbol{R}_\mathrm{cn} = \left[{}^2R_\mathrm{cn,\,x} \quad {}^2R_\mathrm{cn,\,y} \quad 0 \right]^\mathrm{T} \tag{54} $$

- $\boldsymbol{R}_\mathrm{cs}$: reaction force from the bevel gear integral with the shaft and acting along the line of action of the mating gears. Its orientation coincides with axis *z4* in S_4 and its point of application with *O4*.

$$ \begin{aligned} &{}^4\boldsymbol{R}_\mathrm{cs} = \left[0 \quad 0 \quad {}^4R_\mathrm{cs,z} \right]^\mathrm{T} \\ &\rightarrow\ {}^4\boldsymbol{R}_\mathrm{cs} = \mathbf{M}_{24}\,{}^4\boldsymbol{R}_\mathrm{cs} = \mathbf{M}_{21}\mathbf{M}_{14}\,{}^4\boldsymbol{R}_\mathrm{cs} \end{aligned} \tag{55} $$

4.3.3 Equilibrium Equations

Cylinder block translational and rotational (about *O2*) equilibrium equations in coordinate system S_2 are written, in vector notation, as follows:

$$ \begin{aligned} &{}^2\boldsymbol{F}_\mathrm{m} + \sum_\mathrm{k} {}^2\boldsymbol{F}_\mathrm{pf,k} + \sum_\mathrm{k} {}^2\boldsymbol{F}_\mathrm{tp,k} + \sum_\mathrm{k} \left(-{}^2\boldsymbol{R}_\mathrm{c,\,k} \right) + \ \ldots \\ &\ldots + {}^2\boldsymbol{P}_\mathrm{c} + {}^2\boldsymbol{F}_\mathrm{th} + {}^2\boldsymbol{R}_\mathrm{cs} + {}^2\boldsymbol{F}_\mathrm{h} + {}^2\boldsymbol{R}_\mathrm{cn} = 0 \end{aligned} \tag{56} $$

$$ \begin{aligned} &\sum_\mathrm{k} {}^2r_\mathrm{Bk} \wedge \left(-{}^2\boldsymbol{F}_\mathrm{pf,\,k} \right) + \sum_\mathrm{k} {}^2r_\mathrm{Htp} + {}^2\boldsymbol{F}_\mathrm{tp,k} + \ \ldots \\ &\ldots + \sum_\mathrm{k} {}^2r_\mathrm{Ck} \wedge \left(-{}^2\boldsymbol{R}_\mathrm{c,\,k} \right) + {}^2r_\mathrm{Gt} \wedge {}^2\boldsymbol{P}_\mathrm{c} + {}^2r_\mathrm{Hth} \wedge {}^2\boldsymbol{F}_\mathrm{th} \ \ldots \\ &\ldots + {}^2\boldsymbol{T}_\mathrm{cf} + {}^2\boldsymbol{T}_\mathrm{h} + {}^2r_\mathrm{Hcn} \wedge {}^2\boldsymbol{R}_\mathrm{cn} + {}^2r_\mathrm{O4} \wedge {}^2\boldsymbol{R}_\mathrm{cs} = 0 \end{aligned} \tag{57} $$

The system takes the following matrix format (six unknowns ${}^2\boldsymbol{F}_\mathrm{h,\,z}$, ${}^2\boldsymbol{T}_\mathrm{h,\,y}$, ${}^2\boldsymbol{T}_\mathrm{h,\,x}$, ${}^2\boldsymbol{R}_\mathrm{cn,\,y}$, ${}^2\boldsymbol{R}_\mathrm{cn,\,y}$, ${}^4\boldsymbol{R}_\mathrm{cs,\,z}$): $\boldsymbol{A}_\mathrm{t}\,\boldsymbol{X}_\mathrm{t} = \boldsymbol{B}_\mathrm{t}$

5 Simulation

The aforesaid mechanical model, coded in Fortran, gave origin to a dedicated library of specific submodels (see Fig. 9) in the AMESim simulation environment. As to the hydraulic modelling, use has been made of previous research work at FPRL on axial piston pumps (Monacò et al., 2002). Figure 10 reports the complete AMESim sketch assessed for the attainment of simulation results proposed ahead. Basically, the lower portion of the sketch shows icons of mechanical submodels (cylinder block, piston, shaft and spring). Those at the right side permit the assignment of geometric parameters of the portplate and of other pump components. Those to the left evaluate, in turn, flow areas for the suction and delivery side as well as chambers volumes variations. The upper part of the sketch illustrates instead the hydraulic modelling of the unit. Testing conditions for simulations are set at a delivery pressure of p^* and a rotational speed of 1500 rpm, the working fluid (a mineral oil) is at constant tem-perature of 60°C. Table 5.1 collects further informations on pump and fluid characteristics. Fig. 10 shows portplate timing and the instaneous pressure within a cylinder attained from hydraulic simulation. This, along with the complete pressure distribution within pump cylinders, neglecting friction and inertia, beside providing needed informations for the mechanical analysis, represents the basic source for the onset of mutually exchanged forces within the pump unit.

Table 5.1: Informations on pump and fluid characteristics

Pump type	Casappa Strada-BAP 32.63
Pump displacement	63.7 [cm^3/rev]
Max. angular velocity	1600 rpm (@ pmax = 350 bar) 2350 rpm (@ 0 bar)
Number of pistons	5
Fluid	Agip Arnica 46 Kinematic viscosity (@ p^*_r, 60°C) = 41.3 cSt
Portplate integral with pump cover	
Flow rate @ 1500 rpm (ideal value)	95.6 [l/min]
Torque @ p^*_r (ideal value)	278.8 [Nm]

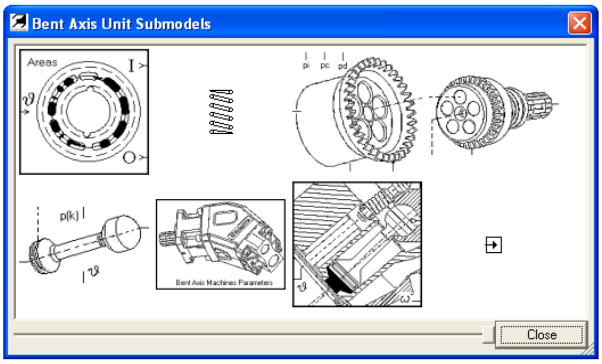

Fig. 9: *Bent Axis Pump Library*

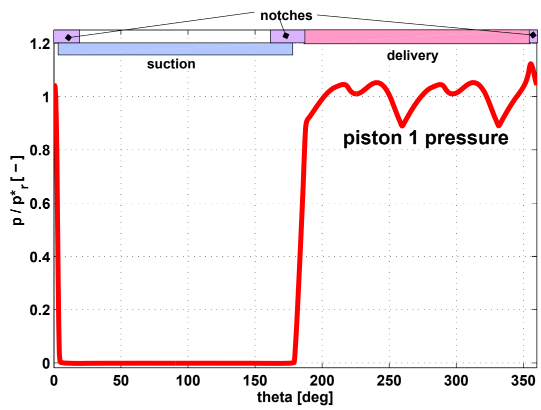

Fig. 10: *Pressure on piston 1*

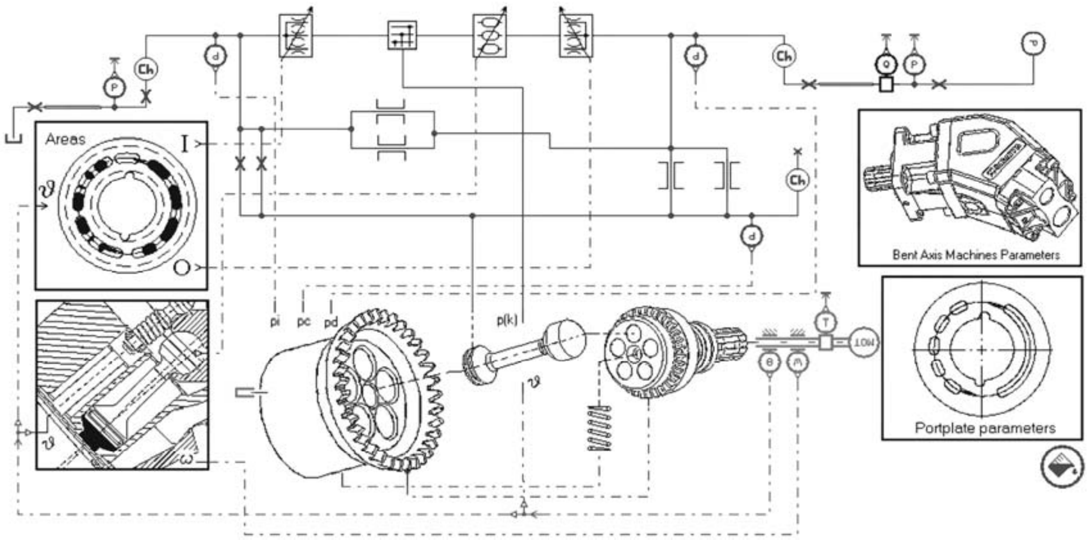

Fig. 11: *Bent axis pump modelling*

5.1 Reactions on Piston

Reaction forces on piston originate from the interaction with the shaft (via the spherical joints) and with the cylinder block. Components of these reaction forces will be considered in coordinate system S_2.

5.2 Reactions between Piston and Shaft

Figure 12 shows, in a complete shaft revolution, the three components of the reaction force ***Rs*** on piston 1[5]: the most significant contribution is along axis *z2* with oscillations about a mean value of 11000 N (delivery phase) that clearly reproduce instantaneous pressure in cylinder 1. It can further be noticed that components along the other two axes, namely *x2* and *y2*, though sensibly smaller, reach nonetheless values that cannot be ignored as both tend to tip the cylinder block. In more detail, Fig. 13(a) demonstrates that when the piston is at the left of axis *z2* (180-360°) ***Rs*** has a negative component along axis *x2* since the piston is so tilted to give always rise to a negative ***Rs*** (*x2*). Along axis *y2* the corresponding component is instead negative in the angular interval 180° to 270° being the piston axis tilted as *r1* in Fig. 13(b); subsequently (from 270° to 360°) it becomes positive (piston axis tilted as *r2*).

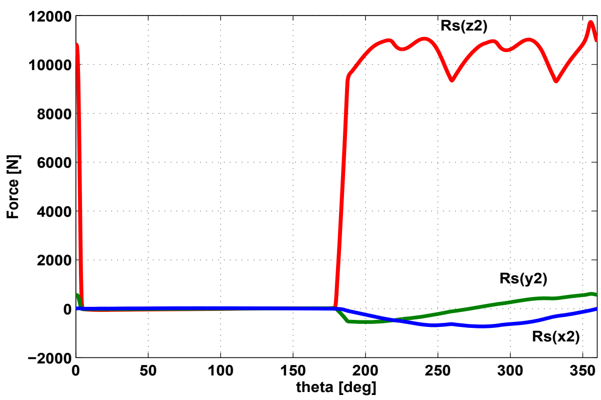

Fig. 12: *Rs: piston-shaft reaction force*

[5] Piston 1 is so identified: at time $t = 0$, it has $\vartheta = 0$ i.e. its point *A* is on the axis *y1* (see Fig. 1, top right).

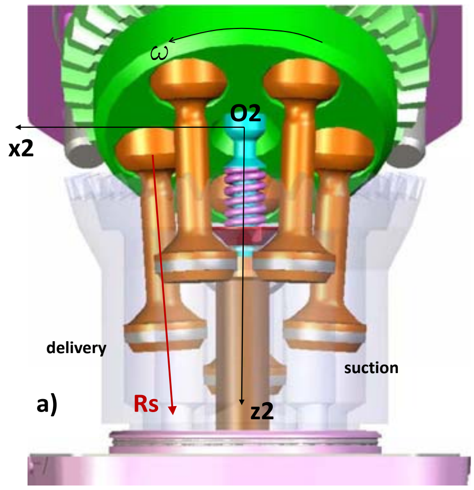

Fig. 13: *Reaction Rs: plane x2-z2 and plane y2-z2*

5.3 Reactions between Piston and Cylinder Block

Figure 14(a) shows components of the reaction force acting on piston 1 from the cylinder block; during suction ***Rc*** essentially balances piston inertia effects. In the delivery phase higher values exist (up to 700 N) as already was the case dealing with shaft reactions. In Fig. 14(b) force ***Fp*** and the two reactions ***Rs*** and ***Rc*** are indicated: in plane *x2 - z2*, their composition is also shown with values corresponding to $\vartheta \approx 280°$ and neglecting inertia.

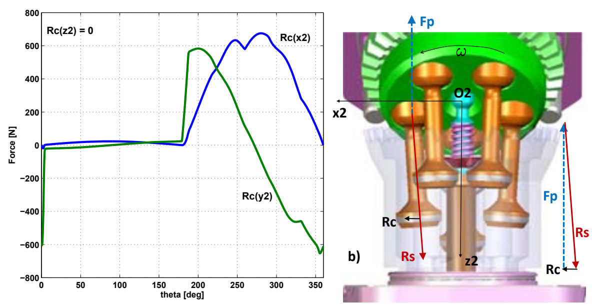

Fig. 14: *Reactions Rc (components) and Rs (plane x2-z2)*

5.4 Reactions on Shaft

Components of these reaction forces will be considered in coordinate system S_1.

5.4.4 Reactions from Bearings

Figure 15 shows, in continuous lines, plots of components in S_1 of the reaction force $\boldsymbol{R}_{b1}$ (tapered roller bearing). Prevailing components act along axes *y1* and *z1* and exhibit comparable magnitude (the shaft is subjected to forces ***Rs*** from pistons (Fig. 16) that have an approximate tilt of 41 degrees with the shaft axis[6]). In addition and with dashed lines Fig. 15 also reports the two components of the reaction force $\boldsymbol{R}_{b2}$ (cylindrical bearing).

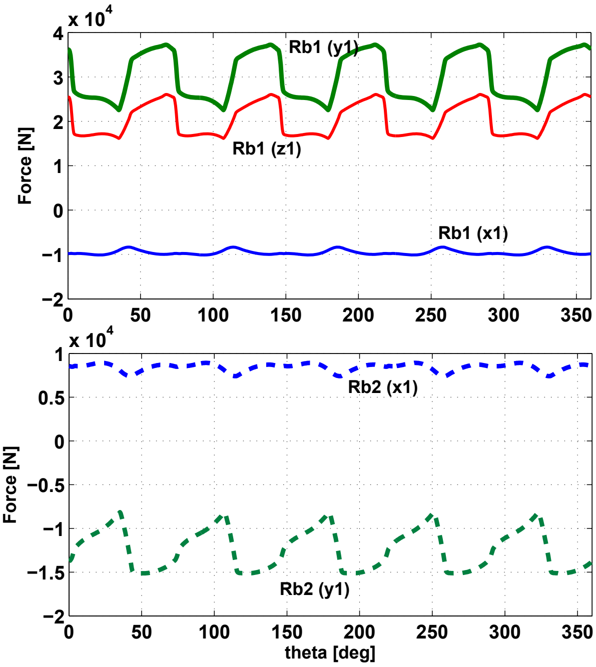

Fig. 15: *Rb1 and Rb2 reactions (components) on shaft*

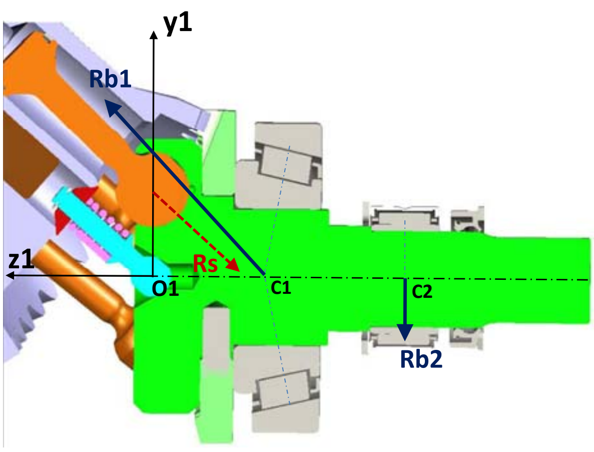

Fig. 16: *Reactions on shaft from bearings*

[6] The model and ensuing simulation take into account the fact that piston axis is not parallel with that of the cylinder.

[7] Piston pressure coincides with the variable chamber pressure. Delivery pressure is instead evaluated in the fixed capacity used to model the delivery volume. In Fig.17 the two traces seem to overlap. In effect the former is higher than the latter since a pressure drop occurs as fluid flows out of the piston chamber through the cylinder block kidney and the portplate.

5.4.5 Pump Torque

Figure 17 shows the instantaneous torque ${}^1\boldsymbol{T}_d$ required to keep the pump running at constant speed, see Eq. 41. At steady state and in one shaft revolution, a number of oscillations equal to the number of pistons is detected; their extent being correlated with delivery pressure (dashed lines, bottom) and, in turn, with the continuously changing pressure inside variable volume chambers (piston 1, full line, bottom)[7]. Figure 18 displays a comparison of experimental torque data with those predicted by the present model. Both are obtained as averages of torque signals sampled over a given time window (1 shaft revolution in simulation and at least 1 s in the test rig). Experimental data acquisition is performed, upon reaching steady-state (1500 rpm), for a number of discrete pump loading conditions (delivery pressure range: 0 - 350 bar).

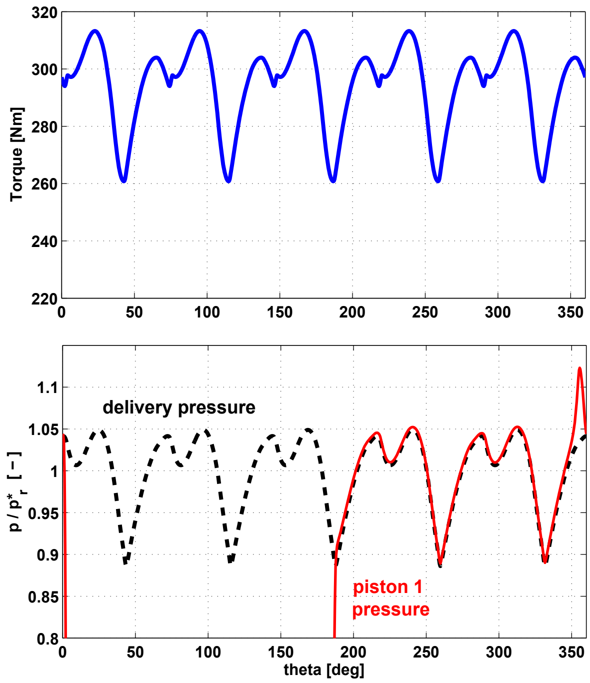

Fig. 17: *Pump torque (top) and pressures (bottom)*

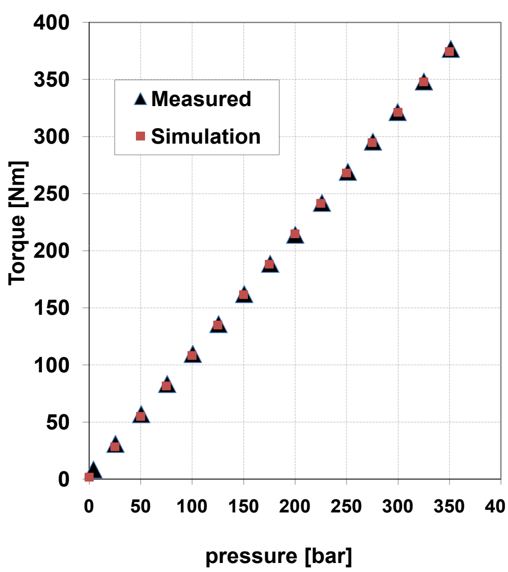

Fig. 18: *Measured and simulated torque*

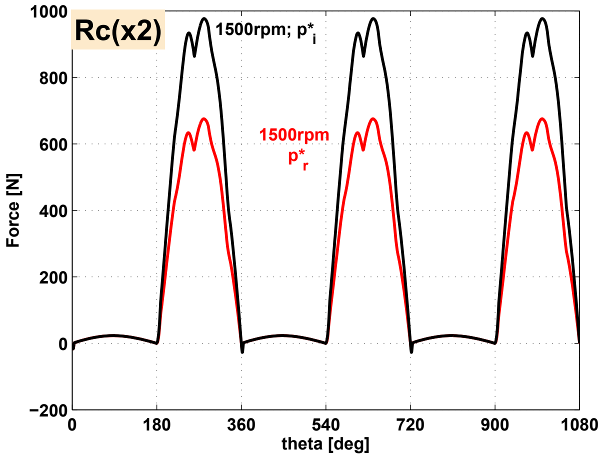

Fig. 19: *Rc reaction, component x2*

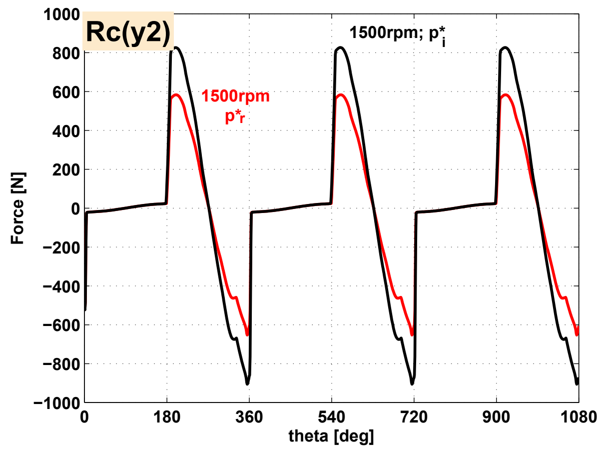

Fig. 20: *Rc reaction, component y2*

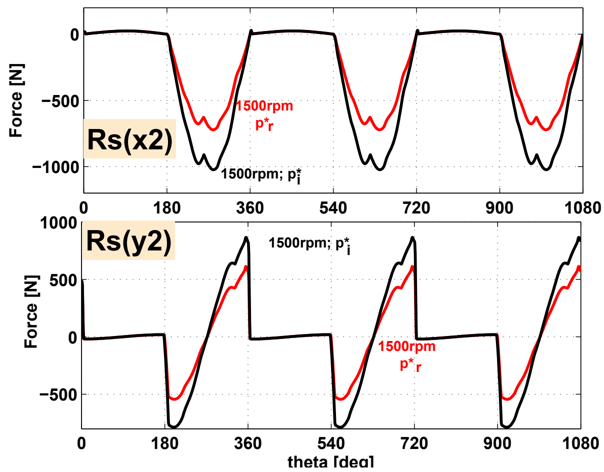

Fig. 21: *Rs reaction, components x2 and y2*

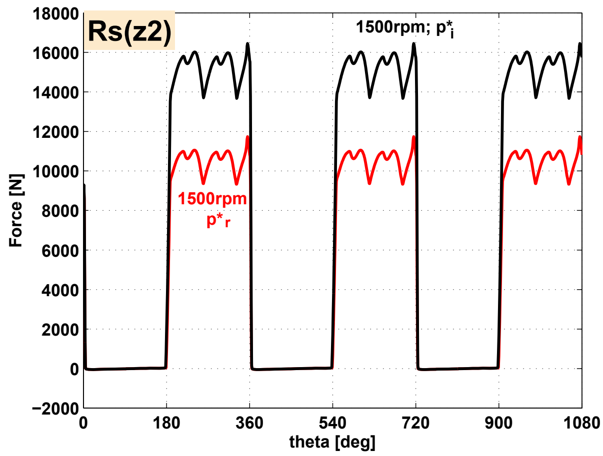

Fig. 22: *Rs reaction, component z2*

6 Influence of Load on Internal Forces

As anticipated, the model easily allows quantitative knowledge of exchanged forces in the pump when different loading conditions are examined. In this respect, a situation is analysed whereby, at constant speed, the unit is operated at peak load (p^*_i). Figure 21 to 24 report predicted results from the present model at 1500 rpm and p^*_i, set against the previously shown case at 1500 rpm and p*. All forces that were considered formerly are now detailed over three shaft turns and, as expected, all increase with load. Worth of notice is the fact that the tapered roller bearing undergoes cyclic component forces (see Fig. 23) surpassing, respectively, 14000 N (Rb1x), 35000 N (Rb1z), and 50000 N (Rb1y). It can further be observed (Fig. 19) that, during suction (see pointing arrow), the reaction ***Rc***(x2) initially rises and then decreases as a consequence of piston acceleration and related inertial effects.

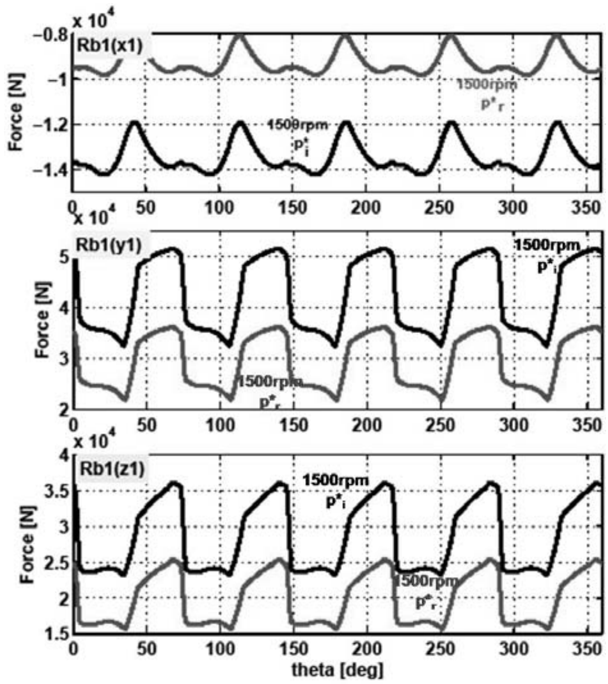

Fig. 23: *Tapered roller bearing reactions (Rb1)*

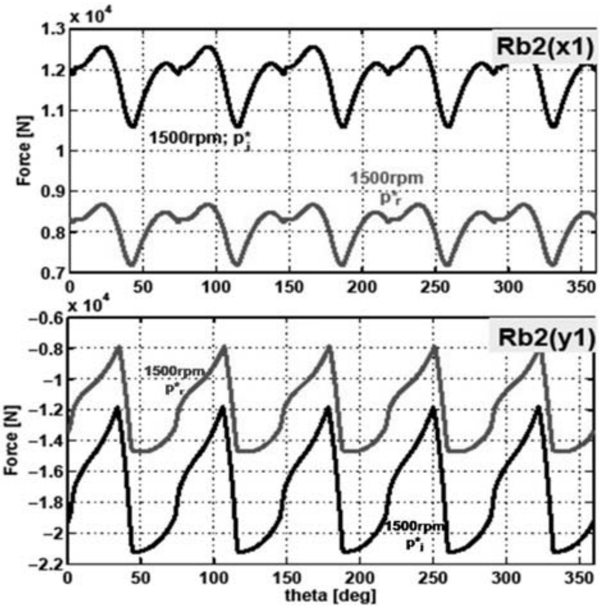

Fig. 24: *Cylindrical bearing reactions (Rb2)*

7 ADAMS Virtual Pump Model

In lack of challenging experimental verifications of the internal forces predicted by the present model one additional investigation is here detailed. This has required the deployment of a full 3-D virtual pump in the ADAMS multibody environment (see Fig. 35). The con-straints assigned are coherent with those used in the mechanical model: i.e. spherical joints (pistons-shaft; tapered roller bearing-shaft), and inline joints (pistons-cylinder block; cylindrical bearing-shaft). External actions on the pump are exerted as follows:

- the instantaneous pressure within variable volume chambers attained in the hydraulic model (Fig. 11) fitted with a spline as shown in Fig. 25, is put to use in ADAMS.
- an angular speed of 1500 rpm is assigned to the shaft.

The ADAMS simulation will ultimately yield the torque required to keep the pump running at steady-state. However, the multibody environment also allows quantitative knowledge, through appropriate measures, of the intervening internal forces. Strip charts of such forces can be monitored while the pump is running and the data stored for appropriate post-processing analysis. Figures 26 to 29 provide a visual cue of ADAMS results contrasted with those achieved utilizing the mechanical model exposed in this paper. Plots of the different reaction forces are nearly identical for the two approaches. Figures 26 and 27 appear, at first sight, as being one the mirror of the other this being false due to the effects of piston inertia. If this contribution were neglected then reactions ***Rc***, ***Rs*** and ***Fp*** would be in equilibrium as shown previously in a simplified scheme in Fig. 14b, where the component along axis *x2* of ***Rc*** equals that of ***Rs***[8].

Figure 30 collects results relative to the evaluation of the instantaneous torque in Adams and in the present model. In the same figure are also reported torque mean values collected from experimental data and predicted in Adams and in the mechanical model. The Adams model, where friction between pistons and cylinder block is neglected, yields a slightly lower mean torque value than the present model. Further, it is also interesting to investigate the torque required from the shaft to transfer rotary motion to the cylinder block through the bevel gears. In this respect, simulations indicate that this originates from two different sources:

- friction effects between the cylinder block and (i) guide pin, (ii) portplate (pump cover), (iii) working fluid in the pump casing. These contributions are modelled through a viscous friction coefficient C, see (47);
- onset of a periodic torque featuring a change in sign and consequent to the balancing effect of reaction forces that pistons exert on the cylinder block.

Figure 32 (top, full line, present model) shows a plot of reaction ${}^4R_{cs,\,z}$ (see Eq. 55) while (bottom, full line, Adams model) shows the torque to be applied to the cylinder block inline joint, where the same shaft velocity is imposed[9]. In both cases an equal viscous friction coefficient value is adopted for the cylinder block: C = 0.0054 Nm/(rev/min) that, at 1500 rpm, originates a constant resistant torque of a 8.1 Nm. Also the situation where this coefficient is supposed to be zero is deliberately considered; though this is not realistic (the and negative sign (the barrel therefore either brakes or barrel rotates fully immersed in a viscous fluid and a accelerates the shaft). It will be demonstrated that this is lubricated gap exists with the fixed portplate) still it consequent to the behaviour of intervening reactions ***Rc*** serves the purpose of highlighting the fact that the shaft-between pistons and barrel. In fact, if this contribution barrel exchanged torque exhibits an alternate positive were absent the situation depicted in the same Fig. 32 with dash lines would be obtained respectively for the force (top) and torque (bottom). Due to the periodic change in sign, both models bring to evidence this specific aspect. In greater detail consider Fig. 31 showing a sufficient to multiply force times the torque front view of the cylinder block: reactions ***Rc*** from pistons onto the cylinder bock are indicated for the angular position ϑ = 0° (circular marker shown in Fig. 32).

[8] In Fig. 14b the polygon of forces has been simplified by omitting the contribution of piston inertia. Owing to this the polygon turns into a triangle of forces. Then, in cited figures, the presence of inertial effects motivate the small but existing difference in components of ***Rc*** and ***Rs***.

[9] To verify if values of the present model are in agreement with those provided by the multibody approach it is sufficient to multiply force ${}^4\mathbf{R}_{cs,\,z}$ times the torque arm; as an example, at $\vartheta = 0$ the present model leads to 329.7 [N] * 0.050023 [m] = 16.49 [Nm] whereas ADAMS to 14.22 [Nm]. As stated, the difference may well be accepted since friction between pistons and cylinder block has been neglected in Adams.

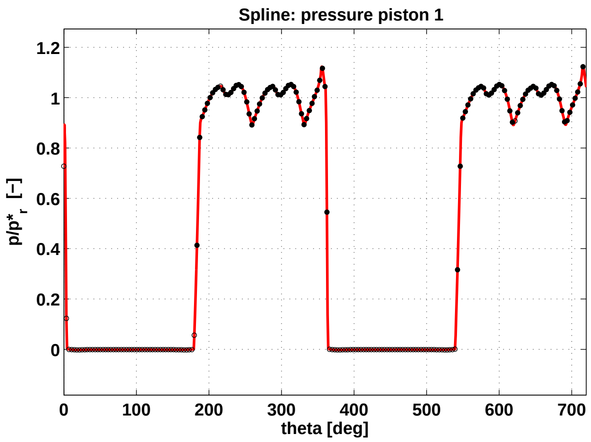

Fig. 25: *Instantaneous pressure within a variable volume chamber (800 points for cubic spline, not all shown)*

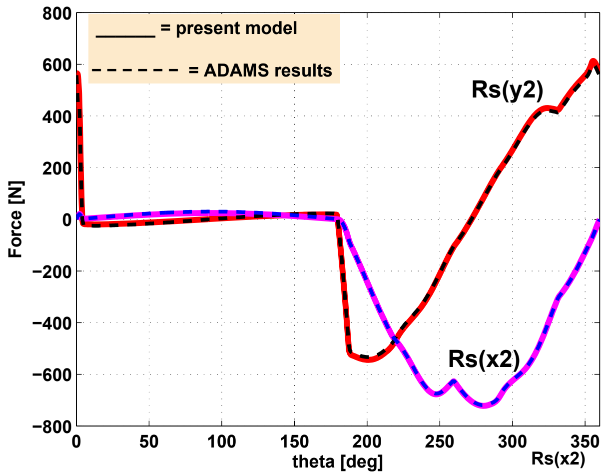

Fig. 26: *Comparison on reactions Rs*

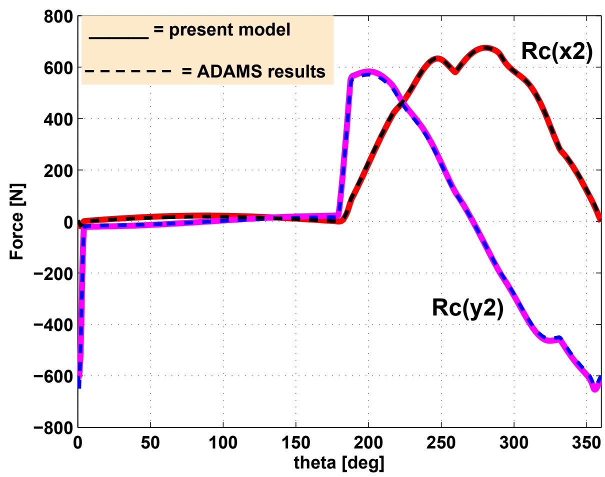

Fig. 27: *Comparison on reactions Rc*

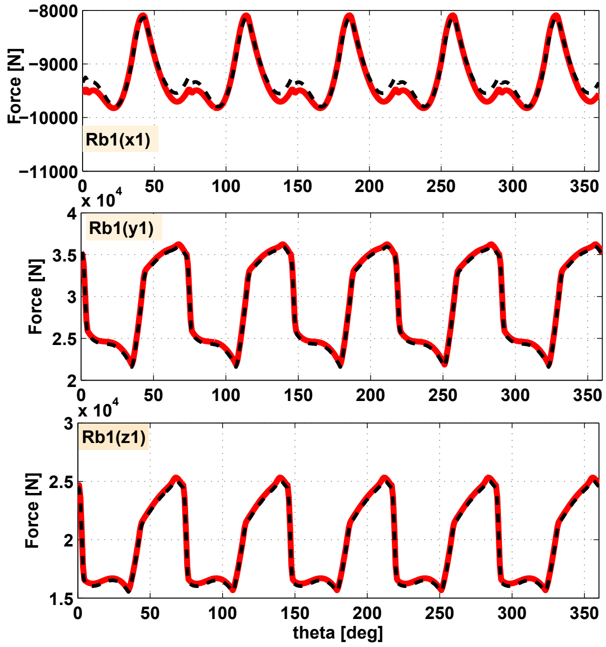

Fig. 28: *Comparison on reactions Rb1*

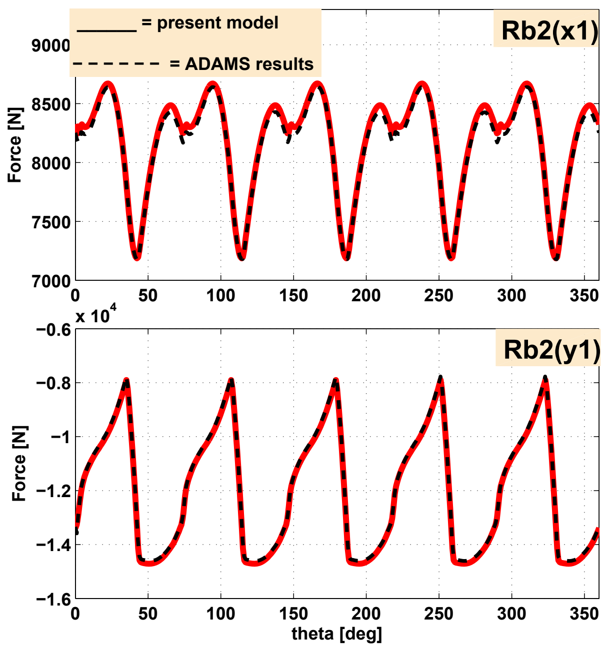

Fig. 29: *Comparison on reactions Rb2*

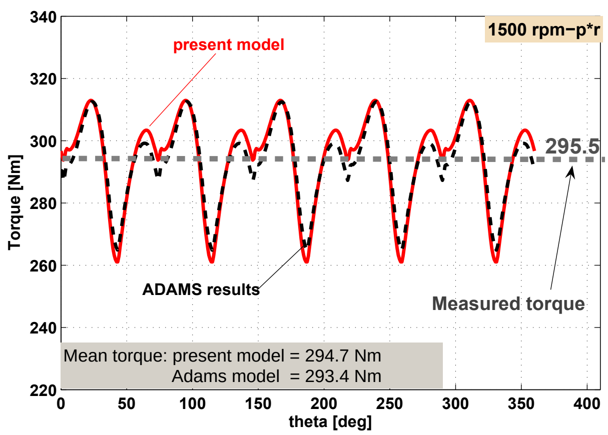

Fig. 30: *Comparison of pump instantaneous and mean torque*

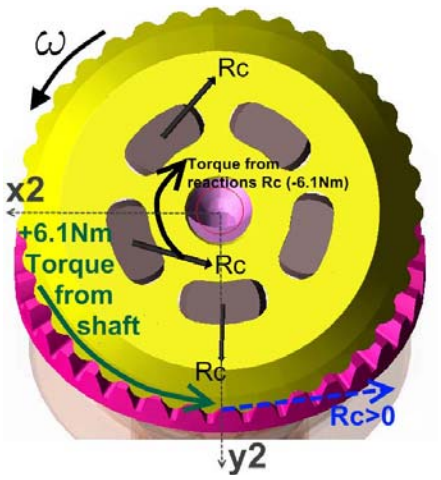

Fig. 31: *Reactions Rc, $\vartheta = 0$*

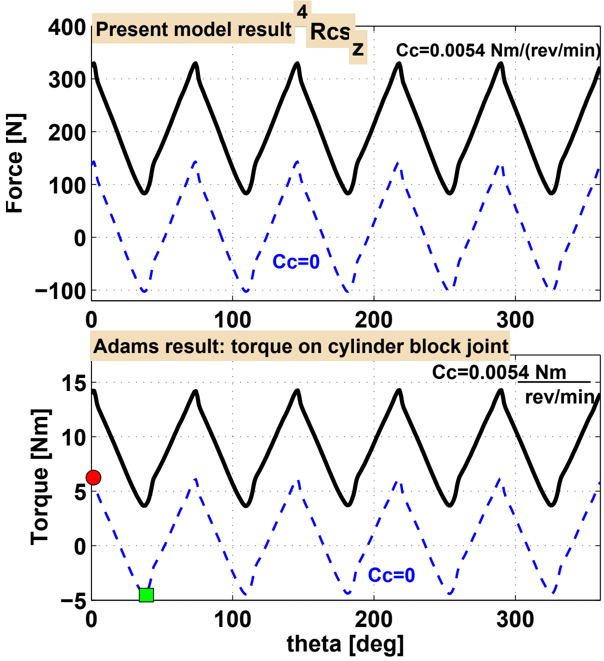

Fig. 32: *Periodic Force and Torque*

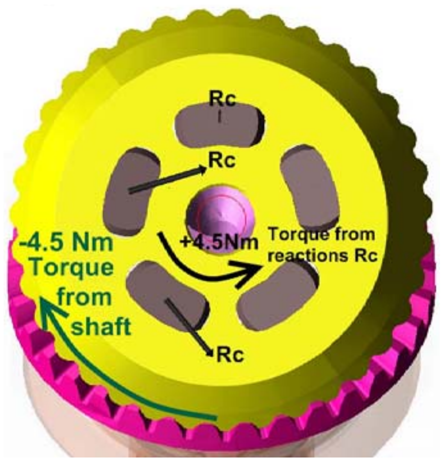

Fig. 33: *Reactions Rc, $\vartheta = 38$*

The resultant negative torque (- 6.1 Nm) acts in the CW direction which is opposite to the shaft angular speed (CCW); consequently in order that equilibrium may be fulfilled the shaft will transfer a positive torque of (+ 6.1 Nm*)* to the block corresponding to a reaction ${}^{4}\boldsymbol{R}_{cs,\,z} > 0$.

On the contrary at $\vartheta = 38°$ Fig. 33 shows that torque (+ 4.5 Nm) acts now in the CCW direction as is the case for ω: equilibrium will then require that the shaft transfers a negative torque. One supplementary check may be obtained through the Adams model by transferring motion from the shaft to the cylinder block through three-dimensional contacts among bevel gears teeth[10] rather than via the inline joint: Fig. 34 shows a plot of reaction $\boldsymbol{R}_{cs}$ (along axis *x2,* see Fig. 31) that demonstrates how its behaviour, similar to that obtained from the present model, clearly reveals the aforementioned periodic change in sign.

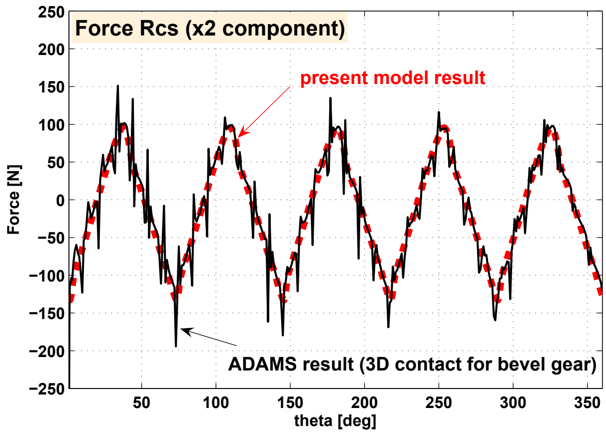

Fig. 34: *Reaction cylinder block-shaft (present model and 3D contacts in ADAMS)*

From what has been written the conclusion may be drawn that, for this type of pump, the torque required to keep the unit turning at constant speed is rather low (Ivantysyn and Ivantysynova, 2000): moments that need be balanced are those stemming from friction, inertia and reactions transmitted from pistons to the cylinder block.

8 Conclusions

This research paper has presented the mechanical model of a fixed displacement bent axis pump. Pump kinematics has been addressed introducing four coordinate systems that were found expedient in the subsequent formulation of needed equations. Interesting peculiarities of piston kinematics have been pinpointed. Modelling phases led to the build up of a dedicated library coded in Fortran and integrated in AMESim to enrich capabilities that were limited to the fluid-dynamics of bent-axis pumps. The only available experimental data were relative to the torque required to drive the unit at constant speed under different loading conditions. Consequently, validation was effected utilizing these data as references and attained results were satisfactory. However, the effort required in modelling also aimed at the evaluation of internal forces ex-

[10] The specific 3D contact algorithm of ADAMS is used.

changed among intervening pump components. In this respect, since specific experimental data were unavailable being, altogether, rather difficult or even impossible to obtain, a full three dimensional virtual model of the unit was assessed in the multibody code Adams. This second approach was used to provide opportunities of performing cross-verifications with the original AMESim predictive results of exchanged forces. Also in this case a fair agreement was confirmed. The AMESim model is, at this stage, more flexible and complete than the ADAMS counterpart also allowing the hydraulic simulation of the pump and its interactions with the circuit it is feeding. Furthermore, being fully parametric, it permits with relative ease to gain quantitative knowledge of the effects entailed by changes in one or several geometric parameters on pump hydraulic and mechanical performance.

On the contrary, the ADAMS model, tied with an imported 3D-CAD geometry of the specific unit, definitely lacks this flexibility. Obviously, at least this restraint, can be subdued by generating anew pump components through purposely written macros (Roccatello et al., 2007), yet at the expense of rather marked efforts.

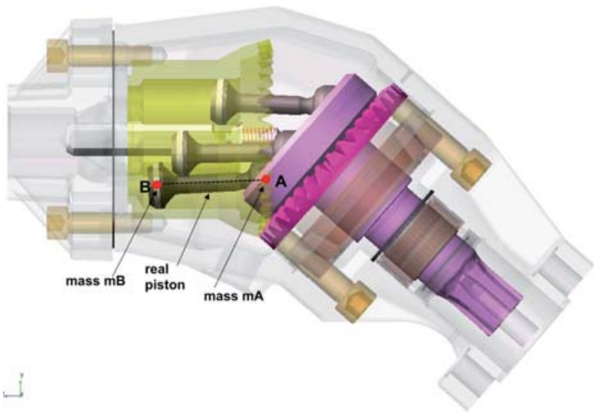

Fig. 35: *ADAMS multibody model*

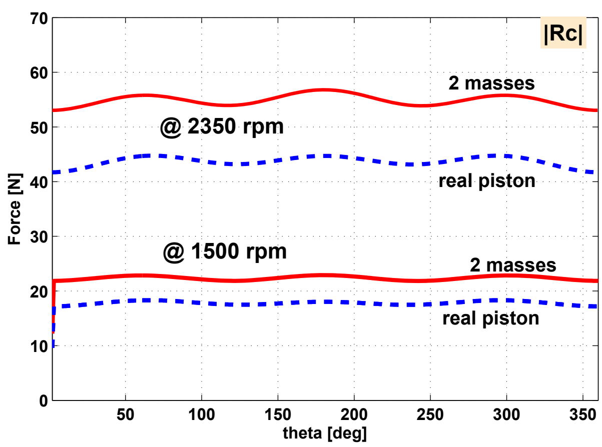

Fig. 36: *Reaction Rc (ADAMS)*

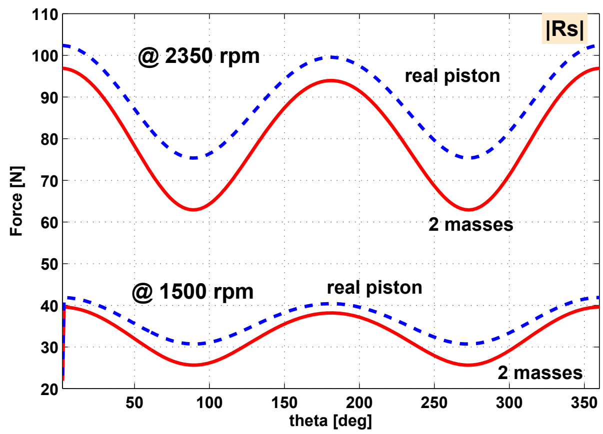

Fig. 37: *Reaction Rs (ADAMS)*

Acknowledgments

The present work has been performed under a research contract with Casappa S.p.A.. Authors acknowledge permission of publishing the present material.

Appendix: Remarks on the Modelling of Piston Inertia

Dealing with piston inertia (subheading 4.1.1) an assumption was made: the piston mass was concentrated in points *A* and *B* with values m_A and m_B. It is then appropriate to verify if this is acceptable or if erroneous approximations in the evaluation of piston-shaft (***Rs***) and piston-cylinder block (***Rc***) reaction forces are introduced. To check this aspect use has been made of the ADAMS multibody pump model (Fig. 35). Two approaches were followed: the first portrays the piston as a massless rod linking two equal masses at points *A* and *B*. The second retains true piston geometry and mass. Constraints are identical and conform with those already explicited in this paper: point *A* attaches to the shaft and the piston (spherical joint); point *B* adapts to the cylinder axis (inline joint). A constant angular speed was applied to the shaft and the pump was run in absence of loads. Fig. 36 confronts the behaviour of ***Rc*** at 1500 and 2350 rpm using the two approaches, whereas Fig. 37 provides the same informations for ***Rs***. Though differences exist (most evident at max rated pump speed), observing that involved forces are at least an order of magnitude smaller than other intervening forces (e.g. see Fig. 14), the hypotheses set forth in the modelling of inertia effects are deemed acceptable.

Nomenclature

A_k	Centre of the spherical piston joint. A
A_c	Area on which cylinder pressure acts
B_k	Centre of the elastic ring
C_c	Viscous friction coefficient (cylinder block rotation)
C_{ij}	Direction cosine
C_k	Point on piston where the reaction force with the cylinder block is applied
C_s	Viscous friction coefficient (shaft rotation)
C_t	Torque loss coefficient (Coulomb friction)
D_{pi}	Cylinder diameter
$\boldsymbol{F}_h$	Hydrodynamic force
$\boldsymbol{F}_{iA,\, k}$	Inertia force (mass lumped at point $\mathbf{A_k}$)
$\boldsymbol{F}_{iB,\, k}$	Inertia force (mass lumped at point $\mathbf{B_k}$)
$\boldsymbol{F}_m$	Spring force
$\boldsymbol{F}_{p,\, k}$	Force from fluid pressure on piston
$\boldsymbol{F}_{pf,\, k}$	Piston-cylinder block friction force
$\boldsymbol{F}_{th}$	Hydrostatic component force pulling the cylinder block away from the portplate (acts at $\mathbf{H_{th}}$)
$\boldsymbol{F}_{tp,\, k}$	kHydrostatic force (acts at $\mathbf{H_{tp}}$)
G_{pi}, G_t, G_s	Piston, cylinder block and shaft centres of mass
$\mathbf{M}_{nm}$	Matrix linking coordinate system m with *n*
N	Number of pistons
O1	Intersection between shaft axis and plane hosting centres of spherical piston joints
O2	Intersection between shaft and cylinder block axes
O4	Point of application of the force exchanged between shaft and cylinder block through bevel gears
O_n, O_m	Origins of 'new' and 'old' coordinate systems (matrix M nm).
P_c ,P_s ,P_{pk}	Cylinder block, shaft and piston weights
Ra	Distance from axis z1 of centres of spherical piston joints
$\boldsymbol{R}_{c,\, k}$	Reaction on piston from cylinder block
$\boldsymbol{R}_{cs}$	Reaction on shaft from cylinder block
$\boldsymbol{R}_{cn}$	Reaction on pin from cylinder block (acts at $\mathbf{H_{cn}}$)
Rd	Distance between cylinder and cylinder block axes
$\boldsymbol{R}_{b1}$ $\boldsymbol{R}_{b2}$	Reactions on shaft from tapered conical and cylindrical bearings (points *C1* and *C2*)
$\boldsymbol{R}_{s,\, k}$	Reaction on shaft from piston *k*
S_m	Coordinate system m
T_d	Drive torque required from prime mover (component along z axis)
$\boldsymbol{T}_{sf}$	Friction torque on shaft
$\boldsymbol{T}_{cf}$	Friction torque on cylinder block
$\boldsymbol{T}_h$	Moment of force Fhy due to its offset position from axis *z2*
$\boldsymbol{T}_{ex}$	Drive torque required from prime mover (vector)
Z	Number of teeth of bevel gears
$\boldsymbol{i}_m, \boldsymbol{j}_m, \boldsymbol{k}_m$	Unit vector of the axes of coordinate system S_m
n a Xq	component along axis q of the acceleration of point X in coordinate system n
b_1	Distance of pointAk from Bk
b	Distance between origins *O1* and *O2*
d	Bevel gears conical pitch diameter
g	Acceleration of gravity
m	Bevel gears module
m_A, m_B	Masses associated with points A_k and B_k
m_s, m_c, m_{pi}	Shaft, cylinder block and piston masses
P_k	Pressure in variable volume chamber of piston *k*
p^*_r	Rated pressure
p^*_I	Intermittent (peak) pressure
nrX, q	component along axis q of the position of point X in coordinate system n
nvX, q	component along axis q of the velocity of point X in coordinate system n
x_m, y_m, z_m	Cartesian axes of coordinate system S
α	Tilt of cylinder block axis with the shaft axis
α_p	Pressure angle in bevel gears
$\delta_{a/t}$	pitch angles in bevel gears
ϑ, ϑ_k	Angular position of piston 1 (ϑ) and piston k
χ	Mass fraction associated with point A
	Angular speed.
k	reference to the specific piston k = 1...N
$[\ldots]^T$	Matrix transponse

References

Caretto, R., **Mancò, S.**, **Nervegna, N.** and **Rundo, M.** 1996. Modelling, Simulation and Experimental Studies on a Variable Displacement Radial Piston Pump Prototype for Automotive Applications. *The ASME International Mechanical Engineering Congress and Exposition*, Fluid Power Systems and Technology, Vol. 3, pp. 1-9.

Fabiani, M., **Mancò, S.**, **Nervegna, N.** and **Rundo, M.** 1999. Modelling and Simulation of Gerotor Gearing in Lubricating Oil Pumps. *SAE International Congress and Exposition*, Detroit, March 1-4, SAE paper 1999-01-0626.

Gad, O., **Rabie, M. G.** and **El-Taher, R. M.** 2002. Prediction and Improvement of Steady-State Performance of a Power Controlled Axial Piston Pump. *Journal of Dynamic Systems, Measurement, and Control*, Vol. 124, Issue 3, pp. 443-451.

Ivantysyn, J. and **Ivantysynova, M.** 2000. *Hydrostatic Pumps and Motors: Principles, Design, Performance, Modelling, Analysis, Control and Testing*. Akademia Books International. ISBN: 185522162.

Jacazio, G. and **Piombo, B.** 1997. *Meccanica applicata alle macchine, Vol. 2*. Levrotto & Bella (Torino). ISBN: 888218014X.

Litvin, F. L. and **Fuentes, A.** 2004. *Gear geometry and applied theory*. Cambridge University Press. ISBN: 0521815177.

Mancò, S., **Nervegna, N.**, **Lettini, A.** and **Gilardino, L.** 2002. Advances in the simulation of axial piston pumps. *Fifth Japan Fluid Power Society International Symposium on Fluid Power*, Vol. 1, pp. 251-258. ISBN: 4931070053.

Mancò, S., **Nervegna, S.**, **Rundo, N.** and **Armenio, M. G.** 2004. Modelling and Simulation of Variable Displacement Vane Pumps for IC Engine Lubrication. *SAE International Congress and Exposition*, Detroit, March 8-11, SAE paper 2004-01-1601.

Manring, N. D. and **Dong, Z.** 2004. The Impact of Using Secondary Swash-Plate Angle Within an Axial Piston Pump. *Journal of Dynamic Systems, Measurement, and Control*, Vol. 126, pp. 65-74.

Roccatello, A., **Mancò, S.** and **Nervegna, N.** 2007. Modelling a Variable Displacement Axial Piston Pump in a Multibody Simulation Environment. *Journal of Dynamic Systems, Measurement, and Control*, Vol. 129, Issue 4, pp. 456-468. ISSN: 0022-0434.

Wieczorek, U. and **Ivantysynova, M.** 2002. Computer Aided Optimization of Bearing and Sealing Gaps in Hydrostatic Machines - The simulation Tool CASPAR. *International Journal of Fluid Power*, No. 1, pp. 7-20.

Alessandro Roccatello
Graduated in Mechanical Engineering (2003) from Politecnico di Torino.After graduation he joined the Fluid Power Research Laboratory of the Politecnico di Torino, focusing on the simulation of axial piston pumps. His research fields are mainly multibody simulation, tribology, axial piston pumps and motors modelling.

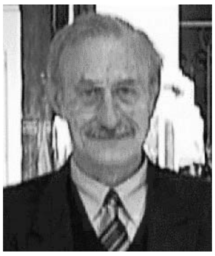

Nicola Nervegna
Graduate in Nuclear Engineering (1971) from Politecnico di Torino, Italy. He joined the Politecnico staff in October 1971 and, at present, is Professor of Fluid Power Systems. His research interests lie in the broad fields of Fluid Power with involvement in positive displacement pumps as well as in the modelling, simulation and testing of various hydraulic components.